

Chapter 3

The Three-Dimensional Phononic Crystals

Badreddine Assouar, Rebecca Sainidou, and Ioannis Psarobas

3.1 Introduction

The conceptual impact of crystalline matter in condensed matter physics has set the framework of understanding the morphological laws of crystals in terms of atomic dynamics. A definite state of atomic equilibrium for an atomic ensemble will necessitate an atomic arrangement in a regular system of points so that the nature of atoms composing the crystal determines under given external conditions their metric disposition, which is summed up in the 230 groups of symmetry. The crystals occurring in nature display the possible types of symmetry enclosed in an abundance of different forms as a result of constitution and environment. The dynamics of the crystal lattice is also responsible for the crystal's physical behavior initiating a connection of outmost importance between quantum mechanics and symmetry. Symmetry plays a great role in ordering the atomic and molecular spectra, for the understanding of which the principles of quantum physics provide the key. An exact classical analogue of a natural crystal is a three-dimensional (3D) phononic

B. Assouar (✉)

International Joint Laboratory (CNRS - Georgia Institute of Technology),
777 Atlantic Dr. NW, Atlanta, GA 30332-0250, USA

Institut Jean Lamour, UMR 7198, CNRS - Nancy University,
Boulevard des Aiguillettes, 54506 Vandoeuvre lès Nancy, France
e-mail: Badreddine.Assouar@gatech.edu

R. Sainidou

Laboratoire Ondes et Milieux Complexes UMR CNRS 6294, Université du Havre, 75 rue Bellot,
76600 Le Havre, France
e-mail: sainidor@univ-lehavre.fr

I. Psarobas

Section of Solid State Physics, University of Athens, Panepistimioupolis,
GR-157 84 Athens, Greece
e-mail: ipsarob@phys.uoa.gr

crystal [28, 35], a composite structure of identical macroscopic scatterers arranged in a 3D crystal lattice points embedded in a homogeneous medium enclosure. Its vibrational spectra is determined by means of multiple elastic-acoustic scattering, a mechanism triggered by interaction with propagating elastic waves of wavelengths comparable to the characteristic size of the crystal (i.e., its lattice constants or else the size of its structured scatterers). It is then evident that by analogy to phononic crystals of lower dimensions, 3D phononic crystals will exhibit as well frequency spectral gaps and in particular omnidirectional elastic wave cutoff behavior [53]. In such a case a well-established topology argument can be stated:

Omnidirectional phononic frequency gaps are favored by cermet topology (a structure of non-touching periodic scatterer arrangement) as opposed to photonic crystals which favor network topology [53].

Since there are striking analogies between the propagation of electrons in crystalline matter and phononic crystals [28], a great variety of multiple-scattering methods (MS) as well as other traditional methods originally developed for electronic-structure calculations have been transferred to the field of acoustics. Thus, the frequency dispersion along the symmetry points in k -space of a phononic crystal, or else known as its phononic band structure, can be calculated by the plane-wave method (PW) [19, 52] and by a more efficient MS method [16] coming from the traditional Korringa–Kohn–Rostoker (KKR) method. On the other hand, well-established purely numerical methods such as the finite-difference-time domain (FDTD) [10], appeared in order to add to the band structure calculations, the computation of the scattering properties (transmission, reflection, and absorption) of finite slabs of a 3D phononic crystal, although it appears to be more effective in 2D problems [62]. In 3D phononic problems, however, the PW method or the FDTD and other finite difference techniques are insufficient to gain physical insight, while in many situations they are computationally cumbersome. The layer-multiple-scattering (LMS) method [37, 46] is a very powerful computational methodology for studying three-dimensional (3D) phononic crystals, a method similar to the layer-KKR developed for low energy electron diffraction (LEED) [27, 28, 33]. An important aspect of the method is that, contrary to traditional band-structure or time-domain methods, it solves the wave equation of elasticity in frequency domain and thus one can allow the elastic coefficients of any of the constituent materials to depend on the frequency, including also absorptive losses of any kind. Besides the complex phononic band structure of an infinite crystal, associated with a given crystallographic plane, the LMS method can also provide the transmission, reflection, and absorption coefficients of an elastic wave of any polarization incident at a given angle on a finite slab of the crystal and, therefore, it can describe an actual transmission experiment. A further advantage of the method is that it does not require periodicity in the direction perpendicular to the layers, which must only

have the same 2D periodicity. Therefore a number of interesting configurations, such as planar defects [38], heterostructures [36], stacking disorder [47], phononic crystal slabs on homogeneous plates and semi-infinite substrates [41] can be treated in a more or less straightforward manner. Finally, the LMS method can incorporate multiple-scattering Green's-function techniques [44] that allow one to calculate the (local) density of states of the elastic field, as well as to treat defects [49], disorder [47], and the system response to an external perturbation [40], in general. The LMS method has been proven very efficient for phononic crystals of spherical particles. It applies to any material type combination (fluid or solid) and with the same efficiency, it can treat, also, coated spheres and generally spherical particles consisting of an arbitrary number of concentric spherical shells by a powerful recursive algorithm [46]. Recently, the method has been extended to scatterers of arbitrary shape with the addition of the extended-boundary-condition (EBC) technique [9, 15]. Thus, in addition to the physical clarity and computational efficiency, the generalized LMS method would offer an efficient and versatile alternative to treat a variety of complex phononic structures. Most aspects of the method will therefore emerge throughout this chapter as the main tool to unfold the physics and applications related to 3D phononic crystals.

We close this part by noting a few words about experiments concerning 3D phononic structures. Although their fabrication is, in general, more difficult and delicate [12, 18, 26] than in the corresponding 2D case, new chemical techniques together with non-destructive measurement methods such as Brillouin light scattering, allowed recently the study of phononic nanostructures operating in hypersonic (GHz) regime, including the case of complex in structure or composition spherical scatterers [5, 57–60]. On the other hand, 3D phononic structures on the macroscale continue to be fabricated and studied experimentally being in very good agreement with LMS theoretical results [25, 30, 61, 65].

3.2 Phononic Lattices

3.2.1 Multiple Scattering and the LMS Method

The essence of any multiple-scattering theory consists in taking into account, explicitly and in an exact and self-consistent manner, all scattering processes occurring in an assembly of scatterers centered on sites \mathbf{R}_n in a homogeneous medium. An outgoing wave from the n 'th scatterer can reach the n th scatterer directly, or indirectly after scattering any number of times by any number of scatterers (including those at \mathbf{R}_n and $\mathbf{R}_{n'}$). We can then generalize the scattering process at \mathbf{R}_n by treating it in two distinct stages. The first stage is described by the individual scattering properties of each scatterer via its scattering matrix, \mathbf{T} , while the second expresses the sum of the contributions to the coefficient of an incident wave on \mathbf{R}_n from all possible scattering paths originating from the outgoing

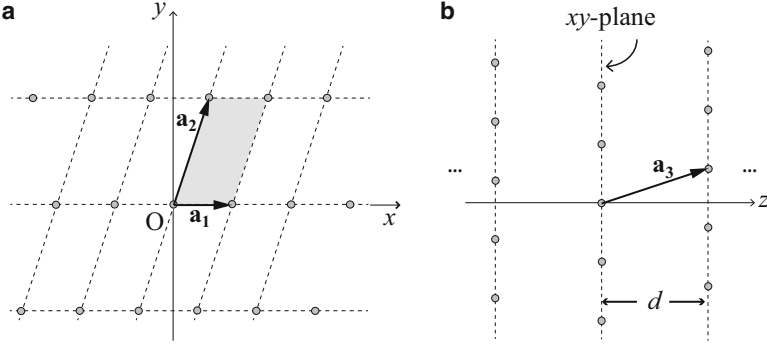


Fig. 3.1 (a) A layer of the crystal consisting of a 2D array of scatterers on xy -plane. (b) The phononic crystal viewed as a succession of identical layers, along z -direction

waves from the other scatterers. The latter is achieved through the introduction of structural Green's functions elements, Ω . The reader may consult [28] for an extended presentation on the matter. Some elements are also given in Sect. 3.3.2.1.

When scatterers are arranged in 3D periodic lattices an efficient and convenient way to perform the multiple scattering is by using the LMS technique. The 3D crystal is viewed as a succession of identical characteristic planes of spheres (layers) of a given crystallographic direction (let's denote it by z -axis direction); each layer has its scatterers arranged in a 2D lattice defined by lattice vectors \mathbf{a}_1 , \mathbf{a}_2 (see Fig. 3.1a), the same for every layer, and is connected to its neighboring layers by a translation lattice vector \mathbf{a}_3 (see Fig. 3.1b), with $d = a_{3z}$ being the distance between consecutive planes of spheres, i.e. the thickness of the layer. By combining several such layers (let's denote their number by N) a finite part of a 3D phononic crystal (slab), of thickness Nd , is formed. We assume a plane wave of angular frequency ω , incident on the slab, with its wavevector component parallel to xy plane, \mathbf{k}_{\parallel} , being a conserved quantity. The LMS finds the exact elastic wave solution layer by layer through the calculation of the four transmission and reflection matrices \mathbf{Q} [37, 46] for each individual layer, by performing the multiple scattering on it; then, it matches the different layers together by combining their \mathbf{Q} -matrices to find the corresponding matrices of the whole composite system. Their knowledge permits the evaluation of the transmittance, reflectance, and absorbance of the slab.

An example of the assembly of spherical scatterers of radius S filling the sites \mathbf{R}_n of a 2D lattice, in particular a square lattice of lattice constant a_0 , is given in the left panel of Fig. 3.2 [42]. Parts (a)–(d) compare theory with experiment [12, 26] to a more than a satisfactory level and thus prove one of the important assets of the LMS method. In Fig. 3.2e, f one can see the evolution of the transmittance through a finite slab of the crystal consisting of N such layers for a longitudinal or transverse wave incident normally on it, with the thickness Nd of the slab. The thicker the slab is, the clearer the regions of frequency where the transmittance practically vanishes, become. For sufficiently thick samples, these regions coincide with the frequency band gaps of the corresponding infinite crystal.

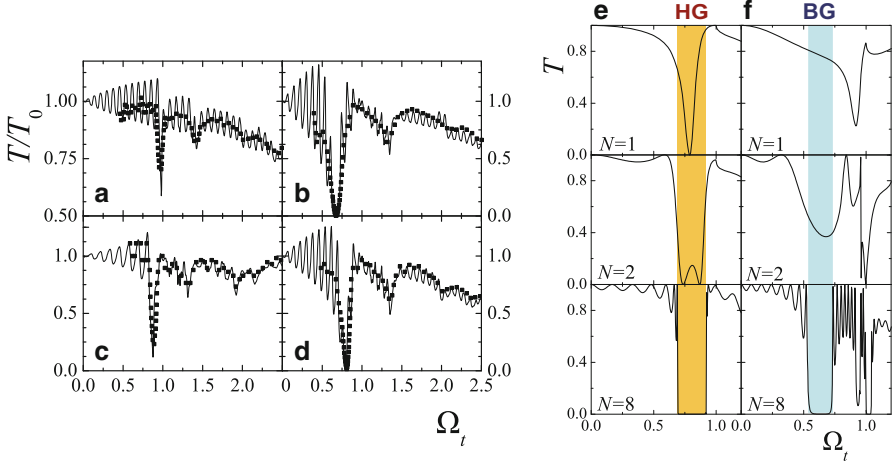


Fig. 3.2 After [42], normalized transmittance for a longitudinal elastic wave incident normally on a square lattice of (a) glass spheres ($S=0.56$ mm, $a_0=2.63$ mm), (b) lead spheres ($S=0.60$ mm, $a_0=2.63$ mm), (c) steel spheres ($S=0.585$ mm, $a_0=3.95$ mm), (d) steel spheres ($S=0.585$ mm, $a_0=2.63$ mm), in the middle of a polyester slab, 7 cm thick, immersed in water. *Solid lines*: theoretical results; *squares*: experimental data. In the *right panel*, we present the transmittance for a longitudinal (e) and a transverse (f) elastic wave incident normally on a slab of N layers of an fcc crystal ($a = a_0\sqrt{2}$ 3.72 mm), parallel to the (001) surface, of steel spheres ($S=0.585$ mm) in an infinite, nonabsorbing polyester matrix. Here $\Omega_t = \omega a_0 / (2\pi c_t)$ and the *shaded areas* denote the gaps of the corresponding infinite crystal, discussed in Fig. 3.3

The complex band structure can be calculated by viewing the infinite crystal as a sequence of layers, extending over all space from $z = -\infty$ to $z = \infty$. After imposing periodic boundary conditions (Bloch's theorem), for a given \mathbf{k}_{\parallel} we determine $k_z(\omega)$ of the 3D wavevector $\mathbf{k} = [\mathbf{k}_{\parallel}, k_z(\omega)]$. This is presented, following Fig. 3.2, in Fig. 3.3a. In general, two types of frequency gaps exist:

- the *Bragg gap* (BG), opening up at the Brillouin zone (BZ) boundaries ($k_z d / \pi = 0, \pm 1$) and originating from the destructive interference of the waves scattered by the periodically arranged layers along a given crystallographic direction. In Fig. 3.3a a BG gap for transverse bands appears about $\omega a / c_t \sim 2\pi$, as shown in Fig. 3.3b. Here and throughout this chapter $c_{l(t)}$ denotes the longitudinal (transverse) elastic velocity in the host matrix, unless otherwise stated.
- the *hybridization gap* (HG), opening up when two bands of the same symmetry cross each other; usually, the most narrow of them originates from virtual bound states localized in the building units (spheres) of the crystal. In Fig. 3.3a the frequency gap for longitudinal bands is a HG, as explained in Fig. 3.3c, d. When a single steel sphere is embedded in polyester, there exists, at $\Omega_t = 0.51$, a virtual bound state (a resonant state of finite lifetime) of the dipole-type displacement field, localized in its interior, as confirmed by calculating

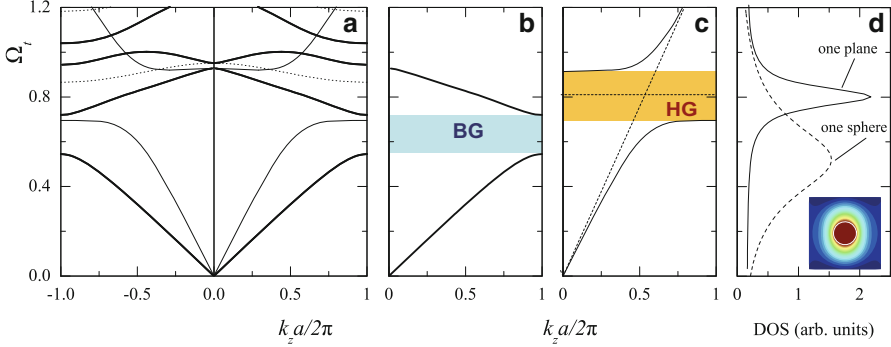


Fig. 3.3 (a) After [42]: The phononic frequency band structure normal to the (001) surface of an fcc crystal ($a=3.72$ mm) of steel spheres ($S=0.585$ mm) in nonabsorbing polyester. The *thin* (*thick*) *solid* lines refer to longitudinal (transverse) bands and the *dotted* lines refer to deaf bands. For the system in (a), we give a schematic representation of (b) a Bragg and (c) a hybridization-induced gap with *solid* (*dotted*) lines showing the hybridized (unhybridized) bands after (before) interaction. In (d) the DOS for one sphere (*dashed* line) and one fcc (001) plane of spheres (*solid* line) for the system under study. In the inset the eigenmode map for a single sphere at resonance, showing strong localization (*red* color) in its interior

the density of states (DOS) by $\frac{1}{\pi} \partial_{\omega} [\text{ImTr} \ln(\mathbf{I} + \mathbf{T})]$ [44]. Next, putting the spheres together to form a layer results in a collective virtual bound state of the longitudinal displacement field, for $\mathbf{k}_{\parallel}=0$, which peaks about the said plane but falls to a much lower value away from it, originating from the interaction of the individual resonant states of the spheres. The corresponding DOS for one layer (an fcc (001) plane of spheres) given now by the formula $\frac{1}{\pi} \partial_{\omega} \{ \text{Im} [\text{Tr} \ln(\mathbf{I} + \mathbf{T}) - \text{Tr} \ln(\mathbf{I} - \mathbf{T}\Omega)] \}$ [44] confirms its existence at $\Omega_t = 0.80$. Therefore, virtual bound states on neighbor planes of spheres will couple weakly with each other, resulting in a relatively flat band as shown schematically in Fig. 3.3c.

It is worthnoting that a HG manifests itself as a dip in the transmission spectrum of a slab even for very thin slabs (monolayers) (see Fig. 3.2e) and does not require any periodicity to exist [57], while a BG appears in the spectrum as a dip progressively by increasing the thickness Nd of the slab, and becomes evident only for sufficiently thick slabs (see Fig. 3.2f).

3.2.2 Formation of Omnidirectional Frequency Gaps, Attenuation, and Tunneling

One of the merits of the LMS method is the reduced \mathbf{k} zone scheme, a surface Brillouin zone (SBZ) which is completely equivalent to the commonly used bulk Brillouin zone (BZ), in the sense that a point in one of them lies also in the other

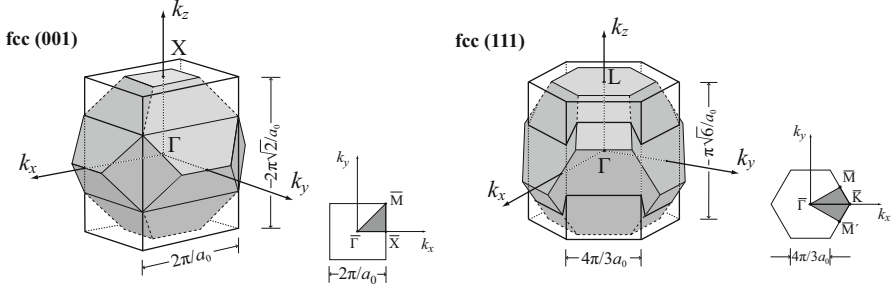


Fig. 3.4 The reduced \mathbf{k} zones associated with the fcc (001) and (111) crystallographic planes and the corresponding SBZ. The bulk BZ is also shown for comparison

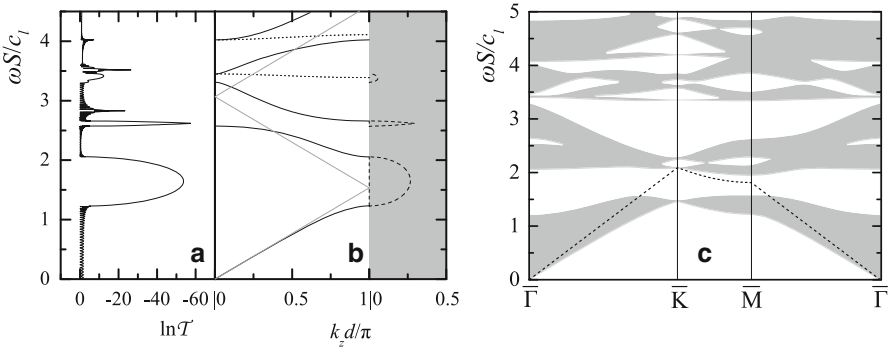


Fig. 3.5 After [45]: (a) Transmittance of a slab consisting of $N = 32$ fcc (111) planes of touching silica spheres in air, at normal incidence. (b) The complex phononic band structure normal to the (111) plane of the corresponding infinite crystal. The *black solid/dotted lines* are bands with Λ_1/Λ_3 symmetry, respectively. The *gray lines* correspond to the effective-medium approximation. Over the frequency gaps, we show by *broken lines* the bands with the smallest imaginary part. The imaginary part is shown in the *shaded region*. (c) Projection of the phononic band structure of an fcc crystal of touching silica spheres in air (volume filling fraction $f = 74\%$) on the SBZ of the fcc (111) surface (see Fig. 3.4), along high symmetry lines. Propagating waves in the air about a slab of the crystal exist for frequencies above a threshold value (a function of \mathbf{k}_{\parallel}) $\omega_{\text{inf}} = c_l |\mathbf{k}_{\parallel}|$ denoted by the *dashed line*

or differs by a vector of the 3D reciprocal lattice (see Fig. 3.4). A full multiple-scattering calculation by means of the LMS method for an fcc crystal of touching silica spheres in air is depicted in Fig. 3.5, where transmission, complex band structure, and the projection on the SBZ of a (111) surface reveal an omnidirectional phononic frequency gap. In this case, together with an extended study of phononic colloidal crystals [39], one can discover interesting symmetry properties of the bands, as well as a clear physical explanation on the origin of hybridization gaps [45, 60].

Absolute spectral gaps do not occur easily in 3D solid phononic crystals. Elastic waves in a 3D solid phononic crystal have longitudinal and transverse components,

and corresponding gaps must overlap, for any direction of propagation, if an absolute gap is to appear. One may think that this is not likely in view of the different propagation velocities of longitudinal and transverse waves. However, under specific conditions, absolute gaps do occur in 3D solid phononic crystals. It has been established that periodic binary composites consisting of nonoverlapping high-density spheres in a low-density host material [17], as well as three-component phononic crystals consisting of coated spheres inside an embedding medium [25], exhibit absolute phononic gaps. The physical origin of the widest of these gaps lies beyond the Bragg gaps at the BZ boundaries: it is a HG. In reality, there are also bands originating from the resonant elastic modes of the individual scatterers: resonant states on neighboring scatterers that couple weakly with each other, resulting in relatively narrow bands, as explained in Fig. 3.3. These bands hybridize with continuum bands of an almost free propagation in an effective homogeneous elastic medium [37, 39, 43]. The opening of the hybridization gap is favored by an increased volume filling fraction, but at the same time it is compromised by the widening of the resonance bands which are also favored by an increased value of the same property of the crystal. This compromising effect will be seized by introducing a mild dissipation on the scatterers of the crystal [34]. In Fig. 3.6, we scan for absolute frequency gaps in a phononic crystal consisting of steel spheres in a polyester matrix with different cubic, tetragonal and in between cases of family arrangements. We show the ratio of the gap width to its respective midgap frequency, $\Delta\omega_G/\bar{\omega}_G$, against the volume fraction f occupied by the spheres. The filling fractions of the above investigation maximize the omnidirectional gap width, at high values of f but below f_{\max} . If we add to the picture a compact arrangement such as the hcp, which has the same $f_{\max} = 74\%$ as the fcc, and the Diamond structure which is not a compact structure, we can draw the following conclusion:

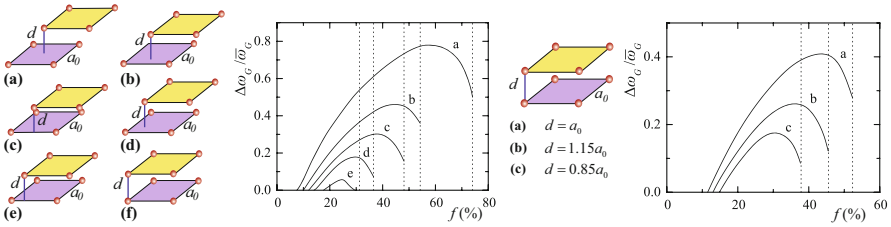


Fig. 3.6 After [43], on the *left panel*, absolute frequency gaps in phononic crystals of steel spheres, centered at the sites of various Bravais lattices specified by the primitive vectors $\mathbf{a}_1 = a_0 (1, 0, 0)$, $\mathbf{a}_2 = a_0 (0, 1, 0)$, and $\mathbf{a}_3 = a_0 (\alpha, \beta, \sqrt{2}/2)$, in a polyester matrix. (a) $\alpha = 0.5$, $\beta = 0.5$ (fcc lattice). (b) $\alpha = 0.5$, $\beta = 0.25$. (c) $\alpha = 0.5$, $\beta = 0$. (d) $\alpha = 0.5$, $\beta = 0.5$. (e) $\alpha = 0.25$, $\beta = 0.5$. The *dotted lines* (normal on the abscissa) indicate the values of f_{\max} corresponding to these structures. For $\alpha = \beta = 0$ (st lattice, $f_{\max} = 26.2\%$) no absolute gap appears. On the right, we present a family of various tetragonal lattices with different interplanar distances d . Note that the sc lattice is the special case when $d = a_0$

Solid–Solid 3D phononic crystals of large density contrast with respect to their embedding medium favor compact structures for the formation of wide absolute spectral gaps. Thus, the geometry of the structure is the most important issue for the formation of omnidirectional phononic gaps in 3D [43].

Damping is an interesting tool in further engineering phononic structures [14] to comply with specific needs in complex applications. An interesting example is the case of an fcc crystal of close-packed rubber spheres in air (see Fig. 3.7). In such a system [34] the induced resonant absorption on the scatterers, and not the host, serves as a cutoff to disturbing resonant states on the frequency spectrum of the phononic crystal, which spoil the formation of clear omnidirectional and partial stop-gaps. This might be extremely useful in relation to waveguiding applications.

Finally, an extended study of finite slabs of 3D phononic crystals with tungsten carbide (or steel) beads embedded in epoxy [30] provided interesting evidence of ultrasonic tunneling and anomalous dispersion of ultrasound near the band edges. Conclusively, in the absence of absorption, the ultrasound tunneling time was found to be independent of the phononic crystal thickness, with $\Delta\omega_{\text{gap}} t_{\text{tun}} \sim 1$ in the middle of the gap (where t_{tun} is the tunneling time and $\Delta\omega_{\text{gap}}$ is the width of the phononic band gap).

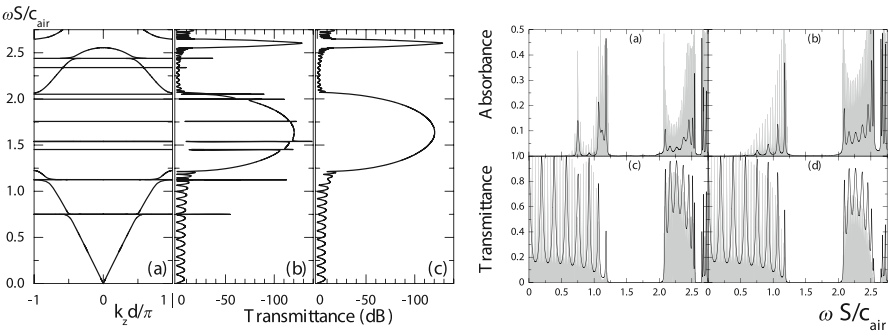


Fig. 3.7 On the *left*: The sonic band structure at the center of the SBZ of a (111) surface of an fcc crystal (of lattice constant a) of close-packed lossless rubber spheres in air. The corresponding transmittance curve of a slab of 16 layers parallel to the same surface is given in the middle. The third graph from the *left* is the same transmittance curve but with spheres of a low viscous level. d is the distance between successive (111) planes of the fcc crystal under consideration. On the *right*: Absorbance and transmittance curves of slabs of the rubber sonic crystal consisting of 8 (*left column*) and 32 (*right column*) planes of spheres, respectively. The *black line* (*shaded curve*) corresponds to the low (high) viscous level. (After [34])

3.2.3 Next-Generation 3D Phononic Structures

The LMS method has been recently extended to nonspherical particles, which are versatile building units for designing functional phononic structures for polarization-selective applications as well as novel acousto-optic devices [9]. A detailed analysis of transmission spectra of such finite phononic crystal slabs by reference to corresponding complex-band-structure and density-of-states diagrams corroborates that nonspherical particles provide an additional degree of freedom for tailoring the modes of the elastic field. There are many applications expected from the effect of distortion of spherical scatterers, an example being single-mode acoustic waveguides based on weakly coupled defects in a phononic band gap crystal. The high degeneracy of the modes of a single spherical defect would imply a large number of bands in the same frequency region within the gap for a chain of such defects. By deforming the spherical shape, a single band could split off, thus ensuring single-mode operation in a given range of frequencies. In Fig. 3.8 we show an example of model phononic crystal consisting of PMMA oblate spheroidal particles.

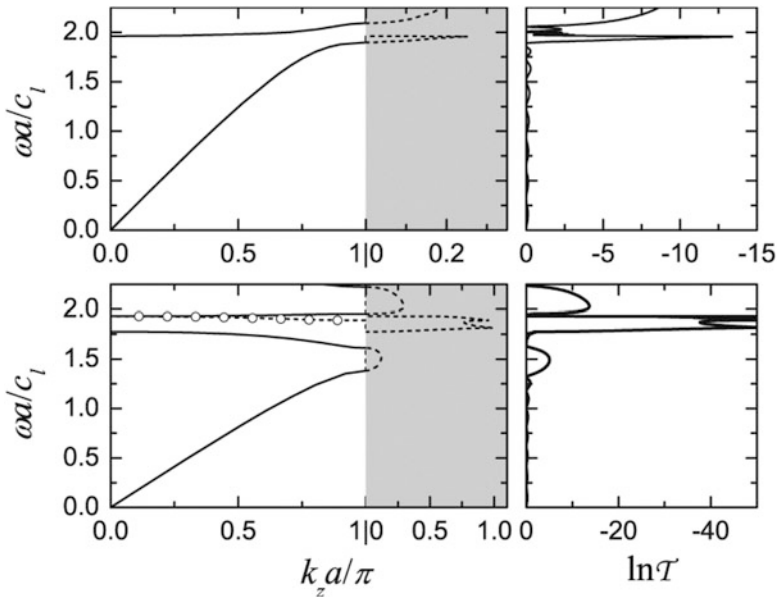


Fig. 3.8 After [9]: (Left panels) The phononic band structure of an infinite sc crystal, with lattice constant a , of PMMA oblate spheroidal particles, with $A = 0.88a$ and $B = 3A/4$, in silicon, along its [001] direction. Over the frequency gaps, we show by broken lines the corresponding complex bands with the smallest in magnitude imaginary part of k_z . The imaginary part is shown in the shaded region. (Right panels) Transmittance of a slab of eight (001) planes of the above crystal at normal incidence for longitudinal (top) and transverse (bottom) incident waves

Classical wave transport in periodic media can provide the means to control light, sound or both with development of phoXonic crystals [31], a special class of dual spectral-gap materials which can integrate the management of sound, light and heat in a versatile manner. Such next-generation structures can operate as dual sensors and they can modulate localized photonic states by hypersound [32, 40] (acousto-optic interactions) or/and create phononic states through optomechanics [6]. In particular, the acousto-optic interaction realized in the merging fields of nanophotonics and nanophonics could lead to unprecedented control of light and sound in very small regions of space [32, 40]. In the regime of inelastic light scattering by sound, one can have phonon-assisted light emission, control of light speed (delay-storage) by stimulated Brillouin scattering and the realization of highly sensitive dual phoXonic sensors. Although it is quite an easy task to realize 1D and 2D phoXonic crystals with omnidirectional spectral gaps, 3D phoXonic crystals were highly unlikely to construct with dual functionality a few years ago, because of the different topology arguments that favor photonic and phononic structures, respectively. Nevertheless, in Fig. 3.9 we present an example of a 3D phoXonic crystal with predicted dual functionality. The phoXonic crystal consists of Au nanospheres in epoxy and for the sc structure at filling fractions above 40 % exhibits an absolute photonic spectral gap of relative width 15 % around the telecom 1.55 μm , as well as an absolute phononic gap of 53 % around the 2 GHz hypersonic frequency.

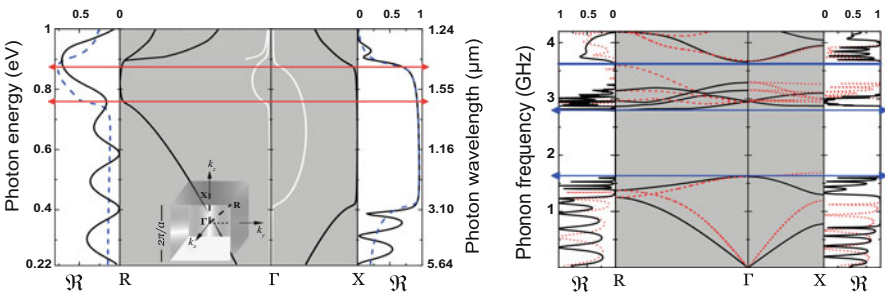


Fig. 3.9 After [31]: (Left panel) Complex photonic band structure and reflectance, \mathfrak{R} , of an sc crystal with lattice constant $a = 480$ nm of Au spheres with diameter 460 nm in an epoxy matrix, along the ΓX and ΓR directions (see inset). The white lines show the imaginary part of the wave vector. The calculation was done with the experimental dielectric function of Au, which includes absorption. Next to the band diagrams we display the corresponding reflection spectra of (001) and (111) slabs of the crystal, five-layers thick, together with the reflectivity of the semi-infinite crystal (dashed lines). The extent of the absolute gap is marked by the horizontal lines. (Right panel) Phononic band structure and reflectance, \mathfrak{R} , of the same crystal along the ΓX and ΓR directions. The solid and dashed lines represent doubly degenerate (shear) and non-degenerate (compressional or deaf) bands, respectively. Next to the band diagrams we display the corresponding reflection spectra of (001) and (111) slabs of the crystal, five-layers thick. Shear (compressional) waves correspond to solid (dashed) lines. The extent of the absolute gaps is marked by the horizontal lines

3.3 Imperfect Phononic Structures: From Periodicity to Disorder

Deviations from periodicity are responsible for several interesting phenomena already encountered in solid state physics and electromagnetic theory, such as Anderson localization of electrons in solids [2], waveguiding, introduction of impurity states within gaps and tunneling, etc. Based on the same principles they are expected, by analogy, to be also found in the case of elastic waves, although the full vectorial character of the elastic problem will add some complexity in the solution of the system.

3.3.1 Layered Non-periodic Heterostructures

As already stated (see Sect. 3.2.1), a perfectly periodic 3D phononic crystal can always be seen as a succession of identical characteristic planes of spheres (layers) of a given crystallographic direction (z -axis), each layer having its scatterers arranged in a 2D lattice (see Fig. 3.1), the same for every layer. Therefore, the simplest way to deviate from periodicity is by letting each layer have its own characteristics: for instance, the size or the material of the spheres and/or the layer thickness, d .

Periodicity can then be destroyed along z -direction (a) *locally* by just introducing some planar (layer) defects [38], (b) *progressively* by changing the layers' characteristics in a smooth manner (following a gradient law [36], or (c) even completely *randomly* by applying a random distribution of size disorder or position disorder (with the fcc stacking faults being the most famous example) [47]. In all these cases periodicity still remains on the 2D lattices parallel to xy plane. We will present them in detail in the next sections.

The LMS is perfectly adapted for the study of such heterostructures, since it performs the multiple scattering on each layer separately, the only restriction being that all layers must have the same 2D periodicity. Therefore, the evaluation of the transmittance, reflectance or absorbance of the composite slab, periodic or not, along z -direction, can be carried out, using the computer code of [46] (all the results shown in this section are obtained by this code).

3.3.1.1 Planar Defects

We take as an example a pure (perfect) crystal consisting of nonoverlapping lead spheres of radius $S = 0.25a$ centered on the sites of an fcc lattice of lattice constant a , embedded in epoxy. An absolute frequency gap extends between $\omega a/c_t = 5.29$ and 7.38. We will show how a slight deviation from periodicity (one impurity plane, i.e. a planar defect, different from the rest) changes dramatically the transmittance

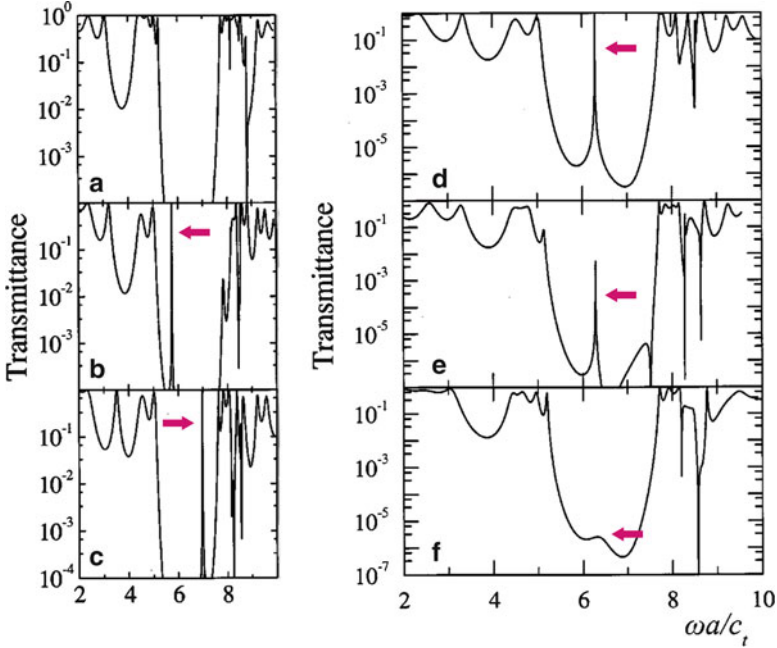


Fig. 3.10 After [38]: Transmittance of transverse elastic waves incident normally on a slab of an fcc crystal of lead spheres in epoxy. The slab consists of five planes of spheres parallel to the (001) surface. *Left:* The spheres have a radius $S = 0.25a$, except those of the middle plane which have a different radius S_i [(a): $S_i = S$, (b): $S_i = 0.8S$, (c): $S_i = 0.6S$]. *Right:* The spheres have a radius $S = 0.25a$, except those of (d) the middle plane, or of (e) the second plane from the surface, or of (f) the surface of the slab, which have $S_i = 0.7S$. Red arrows show the transmission resonance due to impurity planes

of elastic waves incident on a slab of the crystal. A complete study can be found in [38]. When a plane of impurity spheres of radius S_i , bigger or smaller than those of the spheres of the other planes, replaces one of the five (001) fcc planes of a finite slab of such a crystal (see Fig. 3.10a), modes of vibration of the elastic field, localized on this plane, are introduced at frequencies within the frequency gap of the corresponding pure phononic crystal. These show up as sharp resonances in the transmittance of elastic waves incident on a slab of the crystal (see Fig. 3.10b, c). The transmission resonance that now appears at a frequency within the gap signifies the existence of a state of the elastic field centered on the impurity plane: a mode of vibration of the elastic field that extends to infinity parallel to the surface of the slab (in the manner of a Bloch wave), but decays rapidly normal to the impurity plane on either side of it.

The transmission coefficient equals unity at the resonance frequency, when the impurity plane lies in the middle of the slab. When the impurity plane moves away from the middle plane, the transmission coefficient at the resonance frequency becomes less than unity and the resonance disappears altogether when the impurity

plane is removed to the surface of the slab, as demonstrated in Fig. 3.10d–f. Further detailed analysis for phononic-crystal slabs with surface-located impurity planes can be found in [50].

Moreover, a periodic arrangement of impurity planes along a given direction creates narrow impurity bands with a width which depends on the position of these bands within the frequency gap of the pure crystal and on the separation between the impurity planes.

3.3.1.2 Gradient Layered Structures

An example of gradient layered heterostructures is given in [36]. The base phononic crystal is made of mercury spheres embedded in aluminum host and arranged in an fcc lattice of lattice constant a . In such a system absolute gaps appear for filling ratios f between 5.2% and 12.1% and the maximum absolute gap is 2.52% at $f = 8.2\%$, as shown in Fig. 3.11a depicting the width of the gap over the midgap frequency. The full-band-gap feature of the system under study can be enhanced by using a heterostructure containing slabs corresponding to different f (spheres of different size). More importantly, by stacking together seven slabs of different spheres sizes, having consequently overlapping full gaps, one can obtain a resulting $\Delta\omega_G/\omega_{MG} = 14.4\%$ as shown in Fig. 3.11b. In particular, the filling ratios used are 5.9%, 6.3%, 6.8%, 7.5%, 8.23%, 8.93%, and 9.6% (denoted by the vertical lines in Fig. 3.11b). It should be noted that slabs of at least eight planes of spheres are needed in order to preserve with accuracy the full-band-gap feature of the crystal. Therefore a minimum width of $4a$ per slab should be appropriate for stacking and a width of $28a$ for the above heterostructure is recommended at least. We note here that all consecutive (001) fcc slabs have the same 2D periodicity on xy -plane.

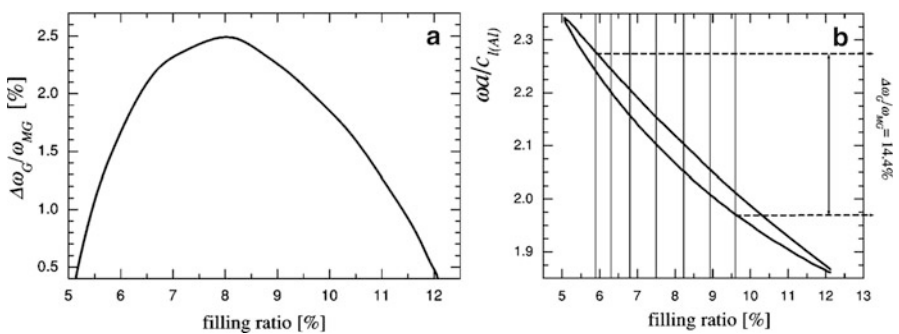


Fig. 3.11 After [36]: (a) The width of the gap over midgap frequency for the fcc crystal of mercury spheres in aluminum as a function of the filling ratio. (b) The edges of the full gap for this crystal as a function of the filling ratio

3.3.1.3 Planar Disorder

We next introduce a random distribution of defect planes along z -direction, having different positions or different sphere sizes with respect to the reference (periodic) phononic crystal.

We first choose for the latter an fcc phononic crystal of steel spheres of radius $S = 0.31a_0$ in a polyester matrix (ordered system I), where a_0 is the nearest-neighbor distance of the crystal and the subindexes l and t refer to longitudinal and transverse wave, respectively. This crystal has an absolute phononic gap extending from $\omega a_0/c_l = 2.32$ to $\omega a_0/c_l = 3.23$ [43]. In Fig. 3.12a we show the frequency band structure normal the (111) surface of the crystal about the region of this gap. Only non-degenerate (longitudinal) bands, denoted by thin lines, are excited when a longitudinal wave is incident normally on a finite slab of the material parallel to the (111) surface; this is not the case for doubly degenerate and deaf bands (thick and dotted lines, respectively). Such a slab of the (ordered) crystal, consisting of a number N of (111) fcc planes of spheres (layers), has thickness Nd (d is the distance between two consecutive planes). When immersed in water and assumed sufficiently thick ($N = 128$ layers), this slab has, as expected, a transmission coefficient (solid line in Fig. 3.12b) practically equal to one over the extension of longitudinal band and vanishing elsewhere, for a longitudinal wave incident normally on it.

Position disorder is next introduced, assuming the simplest case: fcc stacking faults. An fcc slab grown along the [111] direction (let this be the z -direction) consists, in the absence of disorder, of parallel planes of spheres in a sequence: $\dots ABCABC\dots$. The layers A, B, C are identical, having the same 2D periodicity in the xy plane, and each one is displaced relative to the one preceding by $\mathbf{a}_3 = \mathbf{a}_0(1/2, \sqrt{3}/6, \sqrt{6}/3)$ (see Fig. 3.12d). Every time this sequence is destroyed as in $\dots ABC\underline{B}ABC\dots$, we have a stacking fault \underline{B} corresponding to a displacement by $\tilde{\mathbf{a}}_3 = \mathbf{a}_0(-1/2, -\sqrt{3}/6, \sqrt{6}/3)$. The dashed line in Fig. 3.12b gives the ensemble-averaged logarithm of the transmittance, $\langle \ln \mathcal{T} \rangle$, of a normally incident longitudinal wave through a slab, the same as that of the solid line, except that it is disordered by stacking faults with a 20% probability for a stacking fault to appear at each point of the sequence; $\langle \ln \mathcal{T} \rangle$ means averaging over an ensemble of 100 different realizations of random sequences of the given number of layers with a 20% disorder probability. We observe a reduction in $\langle \ln \mathcal{T} \rangle$, relative to the ordered structure at frequencies above and below the edges of the gap, but not a dramatic one. This is due to Anderson localization and to be certain that this occurs, the quantity

$$l/d = -2N/\langle \ln \mathcal{T} \rangle, \quad (3.1)$$

must be independent of N , for sufficiently large values of N . Only then we can refer to l as the localization length. As seen in Fig. 3.12c where l/d is shown for $N = 128$, and $N = 2,048$, l has converged for certain frequencies above the gap (about the edges of the longitudinal band of Fig. 3.12a) which confirms the existence of Anderson localization for these frequencies, for very large samples ($N = 2,048$), without however producing any dramatic difference in the transmission gap.

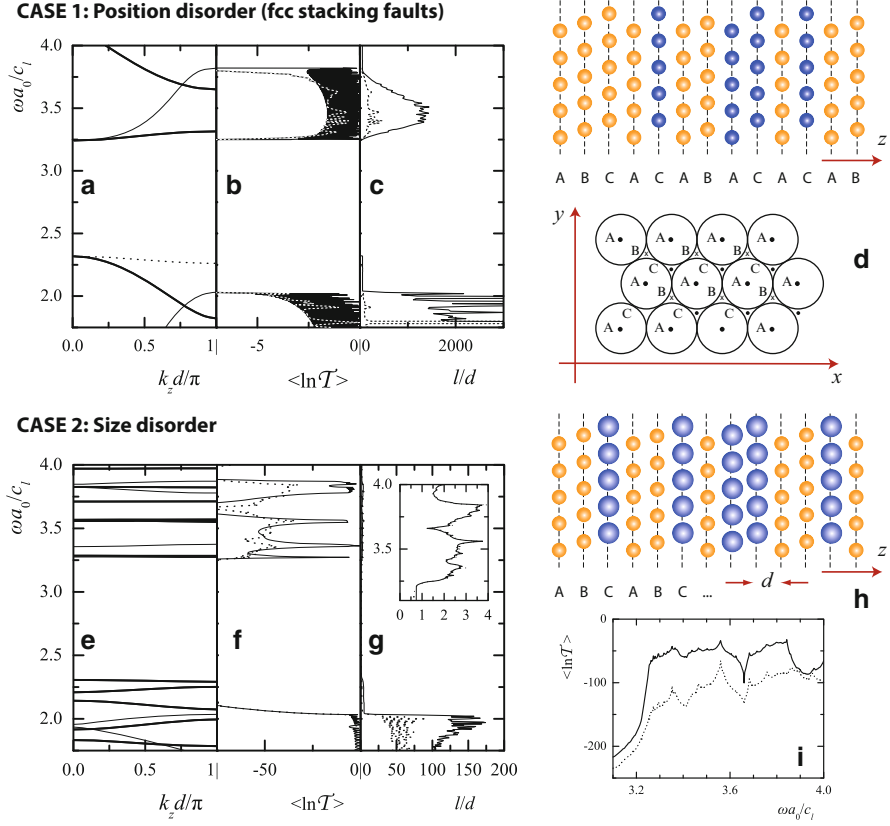


Fig. 3.12 After [47]: *Top panel: Stacking faults. (a)* The frequency band structure along the [111] direction for the ordered system I. *Thin/dotted/thick lines* refer to bands of $\Lambda_1/\Lambda_2/\Lambda_3$ symmetry. *(b)* $\langle \ln \mathcal{T} \rangle$ of a longitudinal wave incident normally on a slab of the material immersed in water. The slab is 128-layers thick and contains 0% (*solid line*) and 20% (*dashed line*) stacking faults. *(c)* l/d for slabs with 20% stacking faults (*dashed line: $N = 128$, solid line: $N = 2,048$*). *(d)* Schematic view of disorder due to fcc stacking faults. *Bottom panel: Size disorder. (e)* The frequency band structure along the [111] direction for the ordered system II. *Thin/thick lines* refer to bands of Λ_1/Λ_3 symmetry. *(f)* $\langle \ln \mathcal{T} \rangle$ of a longitudinal wave incident normally on a slab of the material immersed in water. The slab is 65-layers thick, with 0% (*solid line*) and 20% (*dashed line*) size disorder. *(g)* l/d for slabs with 20% size disorder (*dashed line: $N = 65$, solid line: $N = 256$*). *(h)* Schematic view of size disorder along [111] direction. *(i)* $\langle \ln \mathcal{T} \rangle$ at normal incidence for a slab of system II 64-layers thick, immersed in water, with 20% (*solid line*) and 40% (*dotted line*) size disorder

When size disorder is considered strong Anderson localization occurs leading to considerable widening of the absolute phononic gap. Now the reference crystal (ordered system II) is built as a sequence of fcc (111) planes of spheres as before, except that the last plane in a period of five planes has spheres with a radius $S' = 1.2S$ different from that of the spheres in the rest of the planes ($S = 0.31a_0$).

System II has a period five times larger than that of system I, thus the relatively wide bands about the gap of system I have now to be folded into a reduced zone five times smaller than the original one. This results in a number of narrow bands in system II together with opening of Bragg gaps between them (Fig. 3.12e); the frequency gap of Fig. 3.12a is retained. Comparison of the logarithm of the transmittance of a longitudinal wave incident normally on a slab of this crystal consisting of 65 planes embedded in water (solid line in Fig. 3.12f) to the corresponding $\langle \ln \mathcal{T} \rangle$ of a disordered slab (dashed line in Fig. 3.12f) with 20 % size disorder probability for each plane of the slab to have the larger spheres (Fig. 3.12h) shows a dramatic reduction of the latter over a region of frequency extending well above the frequency gap of the (ordered) crystal. Of course this is due to Anderson localization, as confirmed by the results of Fig. 3.12g: l has converged to a value independent of the thickness for slabs with 65 layers for frequencies above the gap, and more importantly, because the localization length is relatively small (less than the thickness of five layers), slabs of reasonable thickness will now produce the desired effect. At frequencies within the gap, the transmission through the disordered slab remains negligibly small.

Widening of the transmission gap, at least double that of the band gap, due to Anderson localization in such size disordered structures, is favored by the presence of the narrow bands which become easily localized when disorder is introduced. It occurs not only at normal incidence and persists even if water is replaced by polyester on either side of the slab, so that transverse waves are included, i.e. whatever the direction or polarization of the incident wave [47]. Increasing the size disorder (from 20 % to 40 %) leads to further reduction of the transmittance, exponentially at most frequencies (Fig. 3.12i).

3.3.2 Linear Defects

All non-periodic structures presented up to here have retained their periodicity parallel to their characteristic surface, and consequently the LMS technique [37, 46] is perfectly adapted for their theoretical description. However, for point or linear defects or when disorder needs to be extended in 3D, this technique has to be used in its primitive form, i.e. the multiple scattering (MS) has to be performed in the whole space where scatterers exist.

In this section, we will not be extended ourselves to completely random systems. Some work has already been done in bulk (volume) disordered bubbly liquids using multiple scattering techniques (see, for instance, [67]). Recently, random systems composed by solid spheres in a fluid host have been studied experimentally, in ultrasound [11] or hypersound [57] regime, assuming, respectively, position disorder or position and size disorder simultaneously. We note in passing that the case of 3D phononic quasicrystals has been also considered experimentally: they exhibit a “hybrid” behavior between periodic and random structures [61] concerning persistence of both Bragg and hybridization gaps together with reduction

of transmission levels due to localization. A general conclusion could be made here: although the prominent feature of perfectly periodic phononic structures is the appearance of frequency gaps, periodicity is not a precondition for them to exist: hybridization gaps originating from individual resonances localized in the structural units of the system will be still present even when periodicity is removed [57, 61].

We will focus next on the case of linear defects introduced to phononic crystals, directly related to waveguiding. A general description of the multiple scattering in the real space, which of course can be also applied in random media, will be presented first.

3.3.2.1 Multiple Scattering in the Real Space

We will briefly give the principle of the MS in the general case: the inhomogeneities (spheres in our case) are distributed randomly in the space and do not need to be the same. We know that for a homogeneous space a wave of angular frequency ω is transferred from a site n' of position vector $\mathbf{R}_{n'}$ to another site n of position vector \mathbf{R}_n through the so-called propagators of the free space, $\Omega_{nn'}$ (see Fig. 3.13a). On the other hand, each time a wave is incident on a sphere at position \mathbf{R}_n it is diffused by it and the scattering process is described by the scattering-matrix, \mathbf{T}_n^0 , which gives the amplitude of the outgoing wave from that sphere (see Fig. 3.13b). Let's now assume

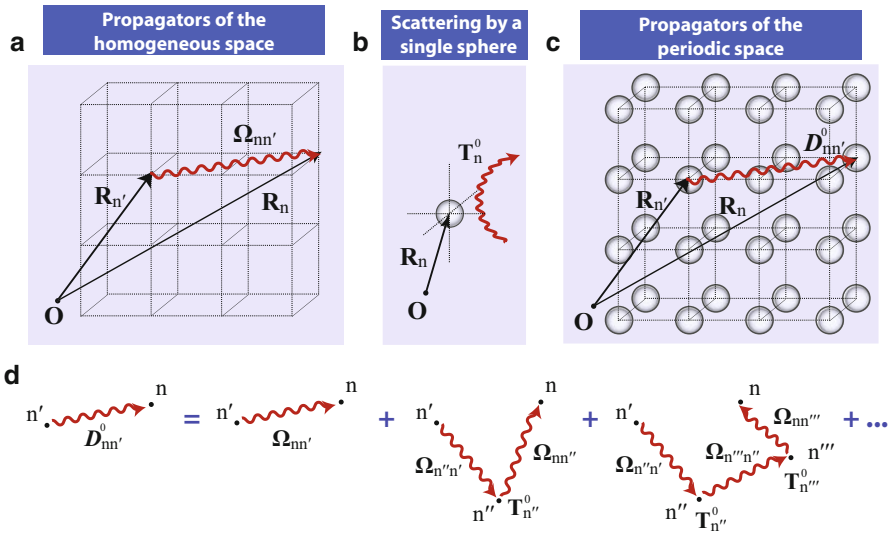


Fig. 3.13 Principle of the multiple scattering in an inhomogeneous medium. (a) Free-host propagator functions describing the propagation of a wave between two sites in the homogeneous space. (b) T-matrix describing the scattering of a wave by an inhomogeneity (*sphere*). (c) Propagator functions describing the propagation of a wave between two sites for a periodic (unperturbed) system. (d) Schematic physical process of propagators based on the multiple-scattering approach

a periodic (unperturbed) system (see Fig. 3.13c) for the purpose we need it later, although what we will present is valid for any type of disorder (in size, material, or position). These two quantities, $\mathbf{\Omega}_{m'}$ and \mathbf{T}_n^0 whose explicit expressions can be found elsewhere [44, 46], are the key for the exact description of the propagation of the wave in that complex system from a site n' to another site n . We need to know the propagators of the complex system, $\mathbf{D}_{m'}^0$, giving the amplitude of the wave incident on the sphere at \mathbf{R}_n due to an outgoing wave from the sphere at $\mathbf{R}_{n'}$. They are the sum of all possible ways (paths) for a wave to travel from n' to n , as shown in Fig. 3.13d: it can propagate directly without any scattering, or after being scattered once, by the site n'' , or after being scattered twice, by sites n'' and n''' , and so on. Thus we can write $\mathbf{D}_{m'}^0 = \mathbf{\Omega}_{m'} + \sum_{n''} \mathbf{\Omega}_{m'n''} \mathbf{T}_{n''}^0 \mathbf{\Omega}_{n''n'} + \sum_{n'',n'''} \mathbf{\Omega}_{m'n''} \mathbf{T}_{n''}^0 \mathbf{\Omega}_{n''n'''} \mathbf{T}_{n'''}^0 \mathbf{\Omega}_{n''''n'} + \dots$ which after an easy matrix manipulation gives [44]

$$\mathbf{D}_{m'}^0(\omega) = \mathbf{\Omega}_{m'}(\omega) + \sum_{n''} \mathbf{\Omega}_{m'n''}(\omega) \mathbf{T}_{n''}^0(\omega) \mathbf{D}_{n''n'}^0(\omega). \quad (3.2)$$

We note here that the superscript “0” in \mathbf{D} and \mathbf{T} refers to unperturbed system to be distinguished from the perturbed one (see below). Equation (3.2) describes in its present form any disorder and/or defect case: we can assume any kind (material and/or size) and any arrangement of spherical scatterers in space. When applied to a periodic system (as we need here), every site n lies on a lattice point and $\mathbf{T}_n^0 = \mathbf{T}^0$ is the same for every point.

We next introduce to the periodic (unperturbed) system some defects (i.e., spheres of different size and/or material) which will be described by a new T -matrix, denoted by \mathbf{T}_n . By analogy to Eq. (3.2) we can then find [44] the corresponding propagator functions for the “perturbed” system, $\mathbf{D}_{m'}$, to be

$$\mathbf{D}_{m'}(\omega) = \mathbf{D}_{m'}^0(\omega) + \sum_{n''} \mathbf{D}_{m'n''}^0(\omega) \Delta \mathbf{T}_{n''}(\omega) \mathbf{D}_{n''n'}(\omega), \quad (3.3)$$

with $\Delta \mathbf{T}_n = \mathbf{T}_n - \mathbf{T}_n^0$, where \mathbf{T}_n is the T -matrix at the site \mathbf{R}_n of the perturbed system and \mathbf{T}_n^0 is that of the original (reference) system. Obviously, the lattice sum of Eq. (3.3) is now restricted only to the sites where the spheres of the reference system have been substituted. The importance of Eq. (3.3) will become more evident in the next section.

We note that all matrices appearing here are defined in $\{P\ell m\}$ space, i.e. including the polarization type P of the waves (one longitudinal and two transverse) and the angular momentum quantum numbers (ℓ, m) used in the spherical-wave expansions of the elastic waves.

3.3.2.2 Waveguiding

Waveguiding in 3D phononic crystals has been very little studied up to now [4, 49]. Waveguides in phononic-crystal structures are usually created by removing a row

(line) of cylinders (spheres), so that the elastic waves of angular frequency ω can be guided through those channels, being reflected on their walls (in analogy to classical waveguides) in condition that ω falls within the frequency region of the absolute gap of the perfect phononic crystal. This type of waveguiding has been widely studied both theoretically and experimentally in 2D phononic crystals, but we know of only one work [4] that transferred this idea in 3D phononic crystals using the FDTD method in a solid/solid composite (lead spheres in epoxy). An alternative mechanism for waveguiding relying on weak coupling through defects along a chain, known as coupled-cavity waveguide (CCW), will be presented here. First proposed in photonic crystals [55], it has been transferred in the acoustic case for a bubbly liquid crystal [49] which supports only longitudinal acoustic waves.

For an efficient waveguiding the operating frequencies must lie within an absolute frequency gap of the phononic crystal. A simple cubic crystal, of lattice constant a , consisting of spherical air bubbles of radius $S_0 = 0.20a$ in water exhibits a wide absolute gap extending from $\omega a/c = 0.087$ to $\omega a/c = 2.228$ (see left panel of Fig. 3.14a), c being the sound velocity in water. This hybridization-type gap originates from the monopole Minnaert resonances of the individual scatterers. The monopole approximation (angular momentum $\ell = 0$ in the spherical-wave expansions of the longitudinal field) compares very well to the exact results obtained by truncating at $\ell_{\max} = 3$ in the said frequency region, as shown in the complex band structure of the above crystal along the [001] direction (see right panel of Fig. 3.14a). Therefore, in what follows, we assume only s -wave scattering (monopole approximation, $\ell_{\max} = 0$).

For the above reasons all matrices related to the multiple-scattering of the previous section will be shrunk to scalar quantities. This system, for the purpose we need it here, allows an exact, almost analytic solution with the consequent physical insight. We calculate from Eq. (3.2) the propagator functions $D_{nm'}^0$ for s waves for the phononic crystal under consideration, where now T^0 is the element of the T -matrix of a single sphere associated with s scattering, having a very simple form [49]; the propagator functions for s waves in the host medium are

$$\Omega_{nm'} = \frac{\exp(iq|\mathbf{R}_n - \mathbf{R}_{n'}|)}{iq|\mathbf{R}_n - \mathbf{R}_{n'}|}, \quad n \neq n' \quad (3.4)$$

with $q = \omega/c$, while by definition, $\Omega_{nn} = 0$. The calculation of $D_{nm'}^0$ on the basis of Eq. (3.2) involves, in general, a summation over a large number of lattice sites because the $\Omega_{nm'}$ decay slowly with the distance $|\mathbf{R}_n - \mathbf{R}_{n'}|$, according to Eq. (3.4). However, the lattice sum in Eq. (3.2) is rapidly convergent at frequencies within an absolute gap because, in this case, the propagator functions $D_{nm'}^0$ decay exponentially with distance, as shown in Fig. 3.14b for a specific frequency at about the middle of the absolute gap of the system under consideration. Moreover, $D_{nm'}^0$ varies practically in isotropic manner and can be well fitted by the function $C \exp(-\beta|\mathbf{R}_n - \mathbf{R}_{n'}|)/(\beta|\mathbf{R}_n - \mathbf{R}_{n'}|)$ for $n \neq n'$, where C is a complex constant [compare here the analogy between $D_{nm'}^0$ and $\Omega_{nm'}$ of Eq. (3.4), when $q = i\beta$]. The value of β obtained from this fit agrees within less than 2 % with the value of $\text{Im}k_z$

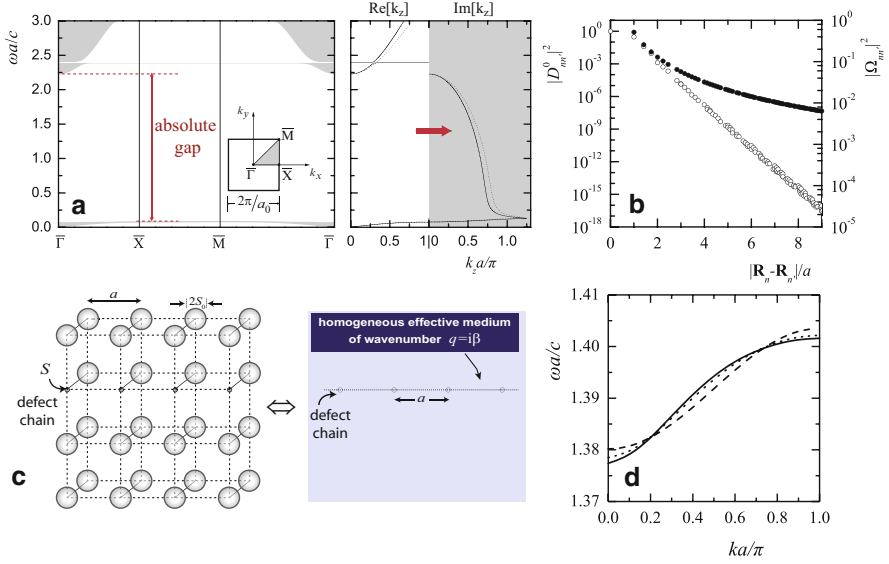


Fig. 3.14 After [49] (a) *Left*: Projection of the phononic band structure of a simple cubic crystal of spherical air bubbles ($S_0 = 0.20a$) in water on the high symmetry lines of the SBZ of its (001) surface (shown in the *inset*). *Right*: The corresponding complex band structure along the [001] direction. In the gap region the $k_z(\omega)$ with the smallest imaginary part is plotted (*shaded area*). *Dotted lines*: monopole approximation. The blank areas correspond to frequency gaps [all $k_z(\omega)$ are complex]. (b) Propagator functions versus distance (*empty circles*), for the crystal in (a) and free-host propagator functions (*filled circles*), both obtained for $\omega a/c = 1.39$ [at about the middle of the absolute band gap shown in (a) by the *red arrow*]. (c) The real waveguide under study (*left*) and its equivalent tight-binding-based description (*right*). (d) Defect band generated by an infinitely long linear chain of defect spheres ($S = 0.01a$) along the [001] direction of the phononic crystal shown in (b). *Solid line*: exact, *dotted line*: nearest-neighbor and frequency-independent propagator approximation. *Dashed line*: best fit to Eq. (3.7). The negative- k section of the band is symmetric to the one shown

at the given frequency (see red arrow in the right panel of Fig. 3.14a). In this respect we can say that *the phononic crystal under consideration behaves, for frequencies within the gap, as a homogeneous and isotropic effective medium characterized by an imaginary wavenumber $i\beta \cong i\text{Im}[k_z(\omega)]$.*

We now introduce the perturbed system by replacing a number of spheres along a line (say along the [001] direction) with bubbles of a different radius $S = 0.01a \neq S_0$ (see Fig. 3.14c). The propagators $D_{nm'}$ for the perturbed system are obtained by solving Eq. (3.3), with $\Delta T_n = T - T^0$, where T and T^0 are the T -matrices for s waves of the perturbed and the original (reference) system, respectively, restricted only to the sites $\mathbf{R}_n = (0, 0, na)$ where defects exist. Note here that $T_n = T$ is independent of n (all defects are taken the same). Taking advantage of the 1D periodicity of this defect chain, Eq. (3.3) is transformed to $D(\omega, k) = [1 - D^0(\omega, k)\Delta T(\omega)]^{-1}D^0(\omega, k)$, where $D^0(\omega, k)$ and $D(\omega, k)$ are the Fourier transforms of $D_{nm'}^0(\omega)$ and $D_{nm'}(\omega)$, respectively. The poles of $D(\omega, k)$ determine the eigenfrequencies of the acoustic

field associated with the chain as a function of k . And since $D^0(\omega, k)$ has no poles over the frequency gap of the unperturbed crystal, these eigenfrequencies are given by the roots of

$$1 - D^0(\omega, k)\Delta T(\omega) = 0 \quad (3.5)$$

for every k in the 1D BZ: $-1 < ka/\pi \leq 1$. The frequency (defect) band of the linear infinite defect chain is calculated from Eq. (3.5) (see solid line of Fig. 3.14d) appearing within the gap. This nondegenerate narrow band results from s modes localized on the defect spheres of the chain interacting weakly between them. We can therefore assume that only nearest-neighbor interaction between the defect spheres matters in Eq. (3.3) and take the relevant propagator functions $D_{mn'}^0$ as constants independent of frequency in the narrow region of the defect band, i.e. put $D_{nn}^0(\omega) \simeq d_0$, $D_{n;n\pm 1}^0(\omega) \simeq d_1$, and $D_{mn'}^0(\omega) \simeq 0$ otherwise. With these approximations, Eq. (3.5) takes the form

$$\frac{1}{\Delta T(\omega)} = d_0 + 2d_1 \cos(ka) , \quad (3.6)$$

which gives indeed very good results (dotted line in Fig. 3.14d).

Here, it is worth comparing the dispersion curve obtained from Eq. (3.6), shown in Fig. 3.14d, with that obtained using a phenomenological tight-binding approach. As already pointed in relation to Fig. 3.14b, for a narrow frequency range about the middle of the gap the crystal can be replaced by an effective homogeneous medium characterized by an imaginary wavenumber $i\beta$ (see Fig. 3.14c), independent of direction and frequency. When a single defect sphere is embedded in it, a localized (about the defect) state of the wavefield appears, decaying as $\exp(-\beta r)/r$ outside the defect sphere, with r the radial distance from its center. The eigenfrequency ω_0 of such a state is given by a pole of the T -matrix for an air bubble in the homogeneous effective medium, and, near the pole we can write $T(\omega) \simeq A/(\omega - \omega_0)$, A being a real quantity. In the case of a chain of spheres in the above effective medium, the wave outgoing from the n th sphere, which behaves like $a_n \exp(-\beta|\mathbf{r} - \mathbf{R}_n|)/|\mathbf{r} - \mathbf{R}_n|$, is generated by the waves incident on it outgoing from the $(n-1)$ th and the $(n+1)$ th spheres (nearest-neighbor approximation). The latter can be expanded about the n th sphere using the $\Omega_{mn'}$ for the effective medium [Eq. (3.4) for $q = i\beta$]. We obtain: $a_n = T(\Omega_{n;n-1}a_{n-1} + \Omega_{n;n+1}a_{n+1})$. For an infinite periodic chain the Bloch theorem requires $a_{n\pm 1} = a_n \exp(\pm ika)$, which leads to the dispersion relation

$$\omega = \omega_0 + 2W \cos(ka) , \quad (3.7)$$

where $W = -A \exp(-\beta a)/(\beta a)$. The values of ω_0 and W in Eq. (3.7) are in general treated as adjustable parameters (leading to the dashed line in Fig. 3.14d) or obtained following the effective-medium approximation as described above [49].

It is worth noting that the same results [Eq. (3.6)] describe the case of a finite chain consisting of N defect spheres, which can also bend any number of times [49].

The above could be generalized to more complicated systems including solid components and whose individual scatterers involve spherical waves of higher angular momentum.

3.4 Multi-component 3D Phononic Crystals (Locally Resonant and Acoustic Metamaterials)

In this section, we first present an overview on 3D locally resonant phononic crystals concerning both 3D bulk systems and finite plates (considered as 2.5D). We next conclude with a short outline on acoustic metamaterials. We will define and describe those types of periodic acoustic materials, and discuss some of their unusual properties, allowing the appearance of new physics phenomena and new appealing applications.

3.4.1 Locally Resonant Phononic Crystals

3.4.1.1 Bulk Structures

During the last decade, the term *Locally Resonant phononic crystals* (LRPC), or sometimes *Locally Resonant sonic materials* (LRSM), established in the pioneer work of P. Sheng and co-workers [25] is tightly associated with systems exhibiting narrow hybridization gaps (HG) at very low frequencies compared to those at which the corresponding Bragg gaps (BG) of the structure occur. We remember here that BG appear at about an angular frequency ω of the order of $\pi c_{l(t)}/a$, a being the lattice period of the structure, and at higher frequencies, which tells us how to choose a if we want a gap in a certain frequency region. On the other hand, the HG originating from localized resonances in the structural units (scatterers) of the system (see relevant discussion in Sect. 3.2.1) open up at frequencies very close to the corresponding resonant eigenfrequencies. The latter (the lower-order mode in an infinite series) occur when the wavelength inside the scatterer is of the order of its characteristic length, i.e. $\lambda_s \sim \Gamma$, Γ being the circumference for the case of spheres. Thus, it is evident that the position of the HG depends strongly on the material(s) and size of the scatterer and is quite robust against structural changes [57], leading to absolute gaps. A proper choice of the constituent materials can therefore tune these HG in a desired frequency region without the need to change the dimensions of the unit cell of the crystal.

P. Sheng and co-workers proposed the use of multilayered spheres within a phononic crystal [24, 25], in particular, scatterers made of a relatively hard elastic core and a soft shell, embedded in an elastically hard host medium, exhibiting localized (in core or shell region) resonant modes which lead to HG in phononic crystals realized from such building components [24, 25, 56]. More precisely for a

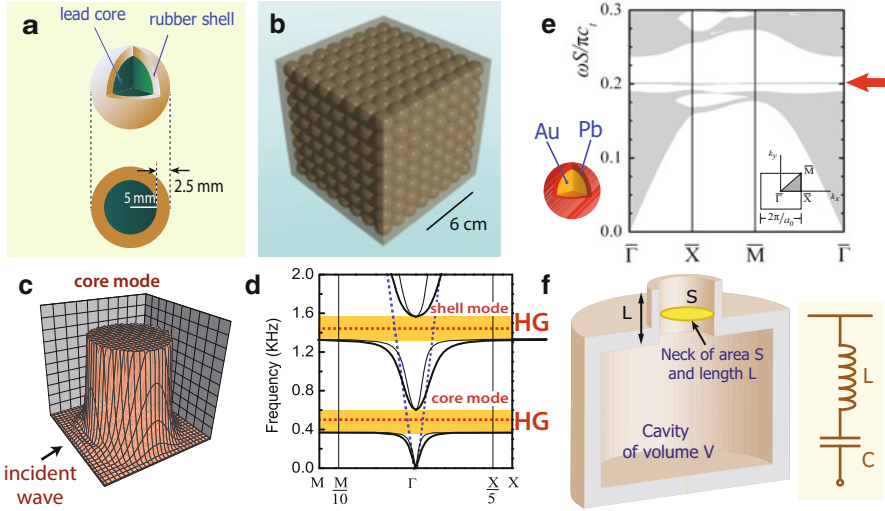


Fig. 3.15 Cross section of a rubber-coated lead sphere (a) that forms the basic structure unit for an $8 \times 8 \times 8$ sonic crystal (b). The core-shell sphere exhibits localized resonances, an example is given in (c), responsible for the appearance of hybridization gaps at very low frequencies, as shown in the calculated band structure (d). Dotted lines denote schematically the unhybridized bands, with the red lines originating from core- or shell-localized resonant states. All results in (c) and (d) were calculated by using the computer code of [46]. (e) An example of LR crystal whose resonant state results in a flat band (red arrow) within an absolute gap. (f) Cross-sectional view of a Helmholtz resonator. A cavity is carved out of a rigid material (gray) and connected to the outside through a neck. The inset illustrates its LC circuit analog. (After [7, 25, 56])

cubic lattice of lead spheres coated by soft silicone rubber and embedded in epoxy matrix (see Fig. 3.15a, b) they managed to obtain narrow HG at wavelengths in the host matrix, λ , two orders of magnitude larger than the lattice constant a [25], as explained in Fig. 3.15c, d. Note here that these wavelengths correspond to the linear dispersion region (long wavelength limit) where the whole crystal can be described, away from the resonances, by an effective homogeneous medium (blue lines in Fig. 3.15d). More importantly, at frequencies close to these HG this linear description is not valid any more and a negative effective behavior for some elastic constants [25] is observed. These frequency ranges can be tuned at will by varying the size and geometry of the structural unit.

Following the same scheme for the multilayered sphere, i.e. hard-soft-hard, but with relatively harder materials than those described above, one can obtain, with an appropriately choice of constituents and shell size, a higher in frequency HG together with a narrow flat band within it, as shown in Fig. 3.15e for the specific case of a phononic crystal of gold-core and lead-shell spherical inclusions in a silicon matrix [24, 56]. This could be very useful in applications such as filtering, waveguiding, etc. More or less the same band structure image (i.e., a flat band originating from localized inside the complex structured scatterer mode) has been

also observed in systems consisting of hollow polymer spheres and cylinders, these resonance modes being tunable up to very low frequencies by varying the shell size [48]. As a remark, we can say that, in general, inclusions of two or more components with an alternation of hard and soft materials act as mass-spring-damper oscillators in each unit cell [7, 20, 24, 25, 48].

We note in passing that, besides multilayered scatterers, a spring-mass behavior can be also achieved by using Helmholtz resonators [7]. They consist of a rigid-wall cavity connected to a fluid matrix through a much narrower neck (see Fig. 3.15f). The fluid in the neck acts approximately as a mass, whereas the compressible fluid in the cavity performs the function of a spring. With the appropriate choice of neck and cavity dimensions, Helmholtz resonators can be made deep-subwavelength at resonance [8]. This type of resonators have not been used up to now in 2D or 3D arrays, as far as we know.

An alternative method to create LRSM without having multicomponent units relies on the use of inclusions with phase speed much lower than that of the matrix [8]. And again, at resonance, the lowest order eigenmodes of an inclusion nominally occur when $\lambda_s \sim \Gamma$, and since $\Gamma \sim a$, we conclude again that in order to have $\lambda \gg a$, a material with very low phase velocity is needed. The most common choice is a soft silicone rubber, which has phase speeds that are two orders of magnitude lower than those of typical solids. Very few studies have considered inclusions consisting entirely of soft rubber [21, 63].

3.4.1.2 Finite Plates

We know of only one work dealing with thin finite slabs of 3D phononic crystals, precisely a square monolayer of polymer spheres placed on a thin glass substrate and immersed in water [41]. In such a system, the resonance modes of the spheres interact with the folded (because of the 2D periodicity) Lamb modes of the plate giving rise to very narrow hybridization gaps (HG) close to the corresponding Bragg gaps (BG). A theoretical study of the several guided and quasi-guided elastic waves together with a group-theory symmetry analysis of the corresponding modes is given in [41], however this structure cannot be typically classified as an LRSM, since the HG do not occur at very low frequencies compared to the BG.

These systems, i.e. thin finite plates containing a 2D array of scatterers along their characteristic surface (instead of spheres we can imagine any type of finite-size scatterers such as cylinders of finite length, disks, ellipsoids, etc.), are usually considered as 2.5D systems, but they remain in fact 3D ones. They attract a lot of interest, since they offer a natural acoustic energy confinement and a simple fabrication [13, 29, 64]. The difference with the corresponding thick finite PC slabs is that now we have to deal with Lamb waves instead of bulk waves.

In order to create locally resonant (thin) phononic slabs we need to choose appropriately their scatterers as described in Sect. 3.4.1.1; we can mainly distinguish two types for these systems: embedded resonators in plates and stubbed plates. An example of the former was reported by T-T. Wu and co-workers who investigated

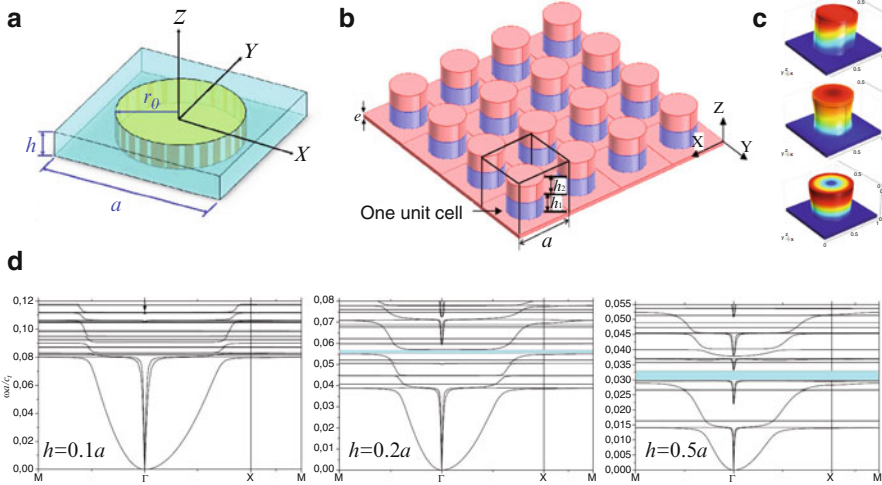


Fig. 3.16 In (a) the unit cell of a PC plate, shown schematically in (b), consisting of cylinder stubs arranged in square lattice. The stubs of radius r and of height h , deposited on a thin epoxy plate, are one-layer (rubber) or two-layer (rubber layer with a Pb cap, with thicknesses h_1 and h_2 , respectively, and $h = h_1 + h_2$). The displacement distribution of some localized modes of different polarization (shear, elongated and breathing modes from *top* to *bottom*) is shown in (c). (d) Band structure for the PC of simple stub, for $r = 0.48a$ and $h = h_1$ varying. (After [13, 29])

a binary LR plate composed of soft rubber inclusions in epoxy matrix (see Fig. 3.16a) [13]. They reported on tuning the low frequency band gap by varying the plate thickness and radius of inclusions. Regarding the LR stubbed plates, binary- and ternary-component LR systems have been recently studied [29, 64]. They are composed, for instance, of simple stubs (silicon rubber) or composed stubs (lead on rubber) (see Fig. 3.16b). The stubs act as spring-mass resonators on a homogenous elastic finite plate and exhibit localized eigenmodes of different polarizations (Fig. 3.16c). These eigenmodes interact with the Lamb modes of the plate resulting in very narrow HG opening up around the corresponding eigenfrequencies, which can be pushed down to extremely low values compared to the frequencies of the BG. Figure 3.16d displays a series of computed band structures showing the opening of HG as a function of the height of stubs. The evolution of the position and width of these HG can be easily explained using a spring-mass model [29]. The LR stubbed plates can be easily fabricated and their physics can be understood more straightforwardly, since we can separately change the effective “spring” constant and the total mass.

The major limitation of locally resonant phononic crystals is their operation only in a narrow frequency regime. To overcome this limitation, we can, as a first step, imagine a 3D system composed of a stack of stubbed plates. The main advantage of this structure besides its potentiality to give a wide LR band gap remains its air/solid composition. A low weight and sturdy 3D structure for sonic regime can then be targeted. The first set of proposed 3D structures (see Fig. 3.17a) are based on rubber

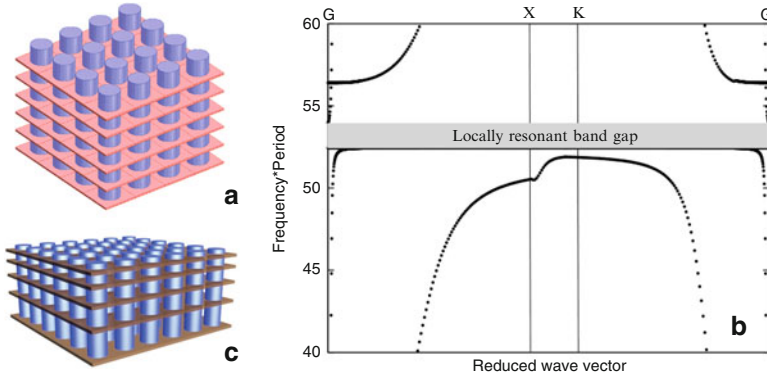


Fig. 3.17 (a) Schematic representation of a 3D LRPC composed of silicone rubber stubs hosted in aluminium frame, whose computed band structure is shown in (b). A complete band gap is observed and *gray shaded*. In (c) an example of a “Gradient” 3D LRPC structure made of silicone rubber stubs on metallic frame

(soft, medium, or hard) stub resonators hosted in a metallic frame (aluminium, steel, brass). The layer-by-layer form of these 3D structures makes their fabrication over a large volume possible. More importantly, they can exhibit omnidirectional (complete) band gaps together with slow sound lines (flat bands). An example is illustrated in Fig. 3.17b for a structure composed of rubber resonators and aluminium plates with a lattice constant of $a = 1$ cm for in-plane and out-of-plane directions; the diameter of rubber resonators is 0.6 cm. The band gap occurs at a normalized frequency of about $fa = 52 \text{ ms}^{-1}$ ($f = 5.2 \text{ kHz}$ for $a = 1$ cm) [3]. The flexibility of this structure enables its engineering by modulating the geometry of phonic crystal in order to achieve more complex structures with desired functionalities. For example, a “gradient structure” can be formed by stacking multiple layers of LR stubbed plates with different thicknesses or periods, as shown in Fig. 3.17c. The principle is the same with the one presented in Sect. 3.3.1.2 for a heterostructure: each layer operating at different frequency range, the whole LR phonic crystal can be, consequently, effective in a large bandwidth. In that manner, wider 3D complete band gaps can be obtained, which can potentially cover the whole desired frequency range for applications such as acoustic isolation or shielding.

Other novel structures are investigated to allow fabrication of wide 3D LR band gap materials, as well. Z. Yang et al. [66] proposed recently a new 3D system composed of stack of different LR membranes called membrane-type acoustic metamaterials. They are composed of an elastic thin membrane extended and fixed by a relatively rigid plastic grid, with a small weight attached at the center of each cell. Figure 3.18a shows a front view of a planar array of the structure. In Fig. 3.18b we show the sound transmission losses (STL) spectra for different samples: two different single membranes, a stack of two membranes and a stack of four membranes. All stacks are composed of different membranes, each one having a different band gap. The transmission of the stacked panel (two membranes)

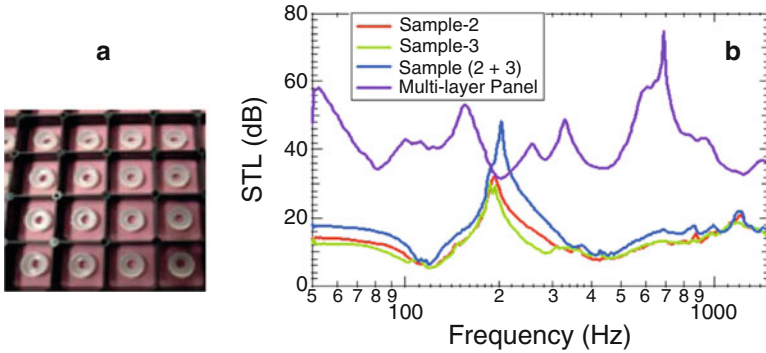


Fig. 3.18 After [66]: (a) Front view of a planar array of square unit cells composing the elastic thin membrane. In (b) some examples of the sound transmission loss of single membranes and of stack of different membranes, each one of them having different band gaps

shows a simple superposition in the individual spectra without any interaction between individual layers, since the membranes spacing (15 mm) is much larger than the evanescent wave decay length (0.8 mm). Broadband shields can therefore be constructed by simply stacking several single-layer panels with strategically selected dip frequencies. In addition, samples with multiweights per cell exhibit multimode vibration patterns and their transmission spectra contain multiple dips, making them advantageous for broadband applications.

3.4.2 Acoustic Metamaterials

Advances in electromagnetic metamaterials [54] offer excellent opportunities to realize new and exotic phenomena, such as negative refraction [51] and artificial magnetism [23]. The acoustic analog of these materials, namely *acoustic metamaterials*, usually includes all those complex media exhibiting unusual properties and thus producing novel phenomena, the most famous, probably, example being that of materials with negative elastic properties [7, 21, 25]. Acoustic metamaterials with LR elements, appropriately designed, is such a case: they can display anomalous response at selected frequencies, leading to negative effective behavior for their elastic parameters [21], which are frequency-dependent and highly dispersive [1]. Therefore, sound waves can be manipulated in surprising ways through such materials, including negative refraction, collimation, focusing, cloaking, sonic screening, and extraordinary transmission [22]. Additionally, these materials can provide a major step toward an effective-medium description, since the spatial periodic modulation of the elastic properties, a , is much smaller than the wavelength in the matrix, λ .

We will briefly describe here a few examples related to some main applications of acoustic metamaterials: negative refraction, focusing, and subwavelength imaging. The first example is related to the negative refraction and focusing in a 3D phononic crystal structure. S. Yang et al. [65] have shown both theoretically and experimentally how a dramatic variation in wave propagation with both frequency and propagation direction leads to novel focusing phenomena associated with large negative refraction. They evidenced that this variation is due to the propagation anisotropy by which the periodic structure “bends” ultrasound beams in unusual ways. The details of the experiment used are illustrated in Fig. 3.19a. A focusing of sound by a 3D periodic acoustic metamaterial was then demonstrated (see Fig. 3.19b, c). On the other hand, experimental evidence of deep-subwavelength imaging using a 2D holey-structured plate was recently reported by Z. Zhu et al. [68]. The basic structure, which consists of a rigid block of brass (impenetrable for sound waves) of thickness h , perforated with deep-subwavelength square holes of side a forming a periodic array with lattice parameter Λ (see Fig. 3.20a), is surrounded by air. They achieved acoustic imaging resolution down to a feature size of $\lambda/50$ (see Fig. 3.20b).

The emergence of LR phononic crystals and acoustic metamaterials, and especially their 3D configurations can offer some new approaches to consider and to deal

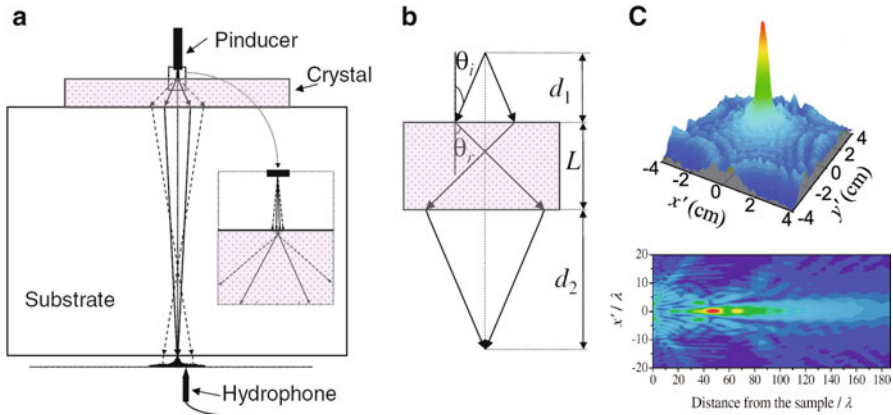


Fig. 3.19 After [65]: (a) Experimental setup, with rays indicating the predicted directions of the group velocity for specific frequency and angles of incidence. (b) Diagram showing the focusing condition in a medium with negative refraction effect. (c) Calculated field plots demonstrating the focusing effect at 1.57 MHz

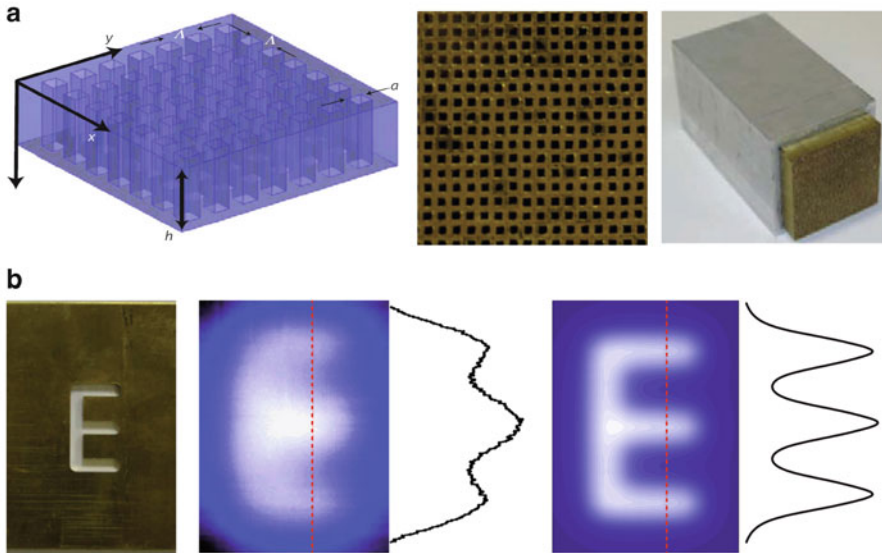


Fig. 3.20 After [68]: (a) Schematic representation (*left*) and top view image (*middle*) of a square array of holes (*square tubes*) drilled in a brass alloy. The holey block is fitted in parallel into 4-inch-wide square aluminium tube and clamped firmly together (*right*). (b) An example of imaging for a deep-subwavelength sized letter “E.” *Left*: the imaging object (letter “E”) of linewidth 3.18 mm, perforated in an ultrathin brass plate. Measured (*middle*) and simulated (*right*) image of letter “E,” obtained at a distance of 1.58 mm from the output plane, together with the acoustic field distribution along the cross-section indicated by the *red dashed line*. The operating frequency is 2.18 kHz ($\lambda = 158$ mm). A $\lambda/50$ linewidth of the object can still be observed in the experiment

with new and appealing applications in low frequency regime. Those materials can present a real added value for a significant breakthrough in some application fields, namely acoustic isolation, seismic shielding, etc.

Acknowledgements R. Sainidou thanks Professors A. Modinos and N. Stefanou for the valuable, enriching, and fruitful collaboration on this topic, from 2000 to 2006.

References

1. M. Ambati, N. Fang, C. Sun, X. Zhang, Surface resonant states and superlensing in acoustic metamaterials. *Phys. Rev. B* **75**, 195447 (2007)
2. P.W. Anderson, Absence of diffusion in certain random lattices. *Phys. Rev.* **109**, 1492 (1958)
3. M.B. Assouar, A. Khelif, A.A. Eftekhar, A. Adibi, Unpublished data
4. H. Chandra, P.A. Deymier, J.O. Vasseur, Elastic wave propagation along waveguides in three-dimensional phononic crystals. *Phys. Rev. B* **70**, 054302 (2004)
5. W. Cheng, J. Wang, U. Jonas, G. Fytas, N. Stefanou, Observation and tuning of hypersonic bandgaps in colloidal crystals. *Nat. Mater.* **5**, 830–836 (2006)

6. M. Eichenfield, J. Chan, R.M. Camacho, K.J. Kerry Vahala, O. Painter, Optomechanical crystals. *Nature* **462**, 78–82 (2009)
7. N. Fang, D. Xi, J. Xu, M. Ambati, W. Srituravanich, C. Sun, X. Zhang, Ultrasonic metamaterials with negative modulus. *Nat. Mater.* **5**, 452 (2006)
8. L. Fok, M. Ambati, X. Zhang, Acoustic metamaterials. *MRS Bull.* **33**, 931 (2008)
9. G. Gantzounis, N. Papanikolaou, N. Stefanou, Multiple-scattering calculations for layered phononic structures of nonspherical particles. *Phys. Rev. B* **83**, 214301 (2011)
10. D. García-Pablos, M. Sigalas, F.R. Montero de Espinoza, M. Torres, M. Kafesaki, N. García, Theory and experiments on elastic band gaps. *Phys. Rev. Lett.* **82**, 4349–4352 (2000)
11. H. Hefei Hu, A. Strybulevych, J.H. Page, S.E. Skipetrov, B.A. van Tiggelen, Localization of ultrasound in a three-dimensional elastic network. *Nat. Phys.* **4**, 945–948 (2008)
12. B.K. Henderson, K. Maslov, V.K. Kinra, Experimental investigation of acoustic band structures in tetragonal periodic particulate composite structures. *J. Mech. Phys. Solids* **49**, 2369–2383 (2001)
13. J.-S. Hsu, T.-T. Wu, Lamb waves in binary locally resonant phononic plates with two-dimensional lattices. *Appl. Phys. Lett.* **90**, 201904 (2007)
14. M.I. Hussein, M.J. Frazier, Band structure of phononic crystals with general damping. *J. Appl. Phys.* **108**, 093506 (2010)
15. S.M. Ivansson, Numerical design of Alberich anechoic coatings with superellipsoidal cavities of mixed sizes. *J. Acoust. Soc. Am.* **124**, 1974–1984 (2008)
16. M. Kafesaki, E.N. Economou, Multiple-scattering theory for three-dimensional periodic acoustic composites. *Phys. Rev. B* **60**, 11993 (1999)
17. M. Kafesaki, M. Sigalas, E. Enonomou, Elastic wave band gaps in 3-D periodic polymer matrix composites. *Solid State Commun.* **96**, 285–289 (1995)
18. V.K. Kinra, E.L. Ker, An experimental investigation of pass bands and stop bands in two periodic particulate composites. *Int. J. Solids Struct.* **19**, 393–410 (1983)
19. M.S. Kushwaha, P. Halevi, L. Dobrzynski, B. Djafari-Rouhani, Acoustic band structure of periodic elastic composites. *Phys. Rev. Lett.* **71**, 2022–2025 (1993)
20. H. Larabi, Y. Pennec, B. Djafari-Rouhani, J.O. Vasseur, Multicoaxial cylindrical inclusions in locally resonant phononic crystals. *Phys. Rev. E* **75**, 066601 (2007)
21. J. Li, C.T. Chan, Double-negative acoustic metamaterial. *Phys. Rev. E* **70**, 055602 (2004)
22. J. Li, L. Fok, X. Yin, G. Bartal, X. Zhang, Experimental demonstration of an acoustic magnifying hyperlens. *Nat. Mater.* **8**, 931 (2009)
23. S. Linden, C. Enkrich, M. Wegener, J. Zhou, T. Koschny, C.M. Soukoulis, Magnetic response of metamaterials at 100 terahertz. *Science* **306**, 1351 (2004)
24. Z. Liu, C.T. Chan, P. Sheng, Three-component elastic wave band-gap material. *Phys. Rev. B* **65**, 165116 (2002)
25. Z. Liu, X. Zhang, Y. Mao, Y.Y. Zhu, Z. Yang, C.T. Chan, P. Sheng, Locally resonant sonic materials. *Science* **289**, 1734–1736 (2000)
26. K. Maslov, V.K. Kinra, B.K. Henderson, Elastodynamic response of a coplanar periodic layer of elastic spherical inclusions. *Mech. Mater.* **32**, 785–795 (2000)
27. A. Modinos, *Field, Thermionic and Secondary Electron Emission Spectroscopy* (Plenum Press, New York, 1984)
28. A. Modinos, N. Stefanou, I.E. Psarobas, V. Yannopapas, On wave propagation in inhomogeneous systems. *Physica B* **296**, 167–173 (2001)
29. M. Oudich, Y. Li, M.B. Assouar, Z. Hou, A sonic band gap based on the locally resonant phononic plates with stubs. *New J. Phys.* **12**, 083049 (2010)
30. J.H. Page, S.X. Yang, Z.Y. Liu, M.L. Cowan, C.T. Chan, P. Sheng, Tunneling and dispersion in 3D phononic crystals. *Z. Kristallogr.* **220**(9–10), 859–870 (2005)
31. N. Papanikolaou, I.E. Psarobas, N. Stefanou, Absolute spectral gaps for infrared light and hypersound in three-dimensional metallodielectric phoxonic crystals. *Appl. Phys. Lett.* **96**, 231917 (2010)
32. N. Papanikolaou, I.E. Psarobas, B. Djafari-Rouhani, B. Bonello, V. Laude, Light modulation in phoxonic nanocavities. *Microelectron. Eng.* **90**, 155–158 (2011)

33. J.B. Pendry, *Low Energy Electron Diffraction* (Academic Press, London, 1974)
34. I.E. Psarobas, Viscoelastic response of sonic band-gap materials. *Phys. Rev. B* **64**, 012303 (2001)
35. I.E. Psarobas, Phononic crystals - sonic band-gap materials (editorial). *Z. Kristallogr.* **220**(9–10), IV (R4) (2005)
36. I.E. Psarobas, M.M. Sigalas, Elastic band gaps in a fcc lattice of mercury spheres in aluminum. *Phys. Rev. B* **66**, 052302 (2002)
37. I.E. Psarobas, N. Stefanou, A. Modinos, Scattering of elastic waves by periodic arrays of spherical bodies. *Phys. Rev. B* **62**, 278–291 (2000)
38. I.E. Psarobas, N. Stefanou, A. Modinos, Phononic crystals with planar defects. *Phys. Rev. B* **62**, 5536–5540 (2000)
39. I.E. Psarobas, R. Sainidou, N. Stefanou, A. Modinos, Acoustic properties of colloidal crystals. *Phys. Rev. B* **65**, 064307 (2002)
40. I.E. Psarobas, N. Papanikolaou, N. Stefanou, B. Djafari-Rouhani, B. Bonello, V. Laude, Enhanced acousto-optic interactions in a one-dimensional phononic cavity. *Phys. Rev. B* **82**, 174303 (2010)
41. R. Sainidou, N. Stefanou, Guided and quasiguided elastic waves in phononic crystal slabs. *Phys. Rev. B* **73**, 184301 (2006)
42. R. Sainidou, N. Stefanou, I.E. Psarobas, A. Modinos, Scattering of elastic waves by a periodic monolayer of spheres. *Phys. Rev. B* **66**, 024303 (2002)
43. R. Sainidou, N. Stefanou, A. Modinos, Formation of absolute frequency gaps in three-dimensional solid phononic crystals. *Phys. Rev. B* **66**, 212301 (2002)
44. R. Sainidou, N. Stefanou, A. Modinos, Green's function formalism for phononic crystals. *Phys. Rev. B* **69**, 064301 (2004)
45. R. Sainidou, N. Stefanou, I.E. Psarobas, A. Modinos, The layer multiple-scattering method applied to phononic crystals. *Z. Kristallogr.* **220**, 848–858 (2005)
46. R. Sainidou, N. Stefanou, I.E. Psarobas, A. Modinos, A layer-multiple-scattering method for phononic crystals and heterostructures of such. *Comput. Phys. Commun.* **166**, 197–240 (2005)
47. R. Sainidou, N. Stefanou, A. Modinos, Widening of phononic transmission gaps via Anderson localization. *Phys. Rev. Lett.* **92**, 205503 (2005)
48. R. Sainidou, B. Djafari-Rouhani, Y. Pennec, J.O. Vasseur, Locally resonant phononic crystals made of hollow spheres or cylinders. *Phys. Rev. B* **73**, 024302 (2006)
49. R. Sainidou, N. Stefanou, A. Modinos, Linear chain of weakly coupled defects in a three-dimensional phononic crystal: A model acoustic waveguide. *Phys. Rev. B* **74**, 172302 (2006)
50. R. Sainidou, B. Djafari-Rouhani, J.O. Vasseur, Surface acoustic waves in finite slabs of three-dimensional phononic crystals. *Phys. Rev. B* **77**, 094304 (2008)
51. R.A. Shelby, D.R. Smith, S. Schultz, Experimental verification of a negative index of refraction. *Science* **292**, 77 (2001)
52. M. Sigalas, E.N. Economou, Elastic and acoustic wave band structure. *J. Sound Vib.* **158**, 377 (1992)
53. M. Sigalas, M. Kushwaha, E.N. Economou, M. Kafesaki, I.E. Psarobas, W. Steurer, Classical vibrational modes in phononic lattices: theory and experiment. *Z. Kristallogr.* **220**, 765–809 (2005)
54. D.R. Smith, J.B. Pendry, M.C.K. Wiltshire, Metamaterials and negative refractive index. *Science* **305**, 788 (2004)
55. N. Stefanou, A. Modinos, Impurity bands in photonic insulators. *Phys. Rev. B* **57**, 12127 (1998)
56. N. Stefanou, R. Sainidou, A. Modinos, Low-frequency absolute gaps in the phonon spectrum of macrostructured elastic media. *Rev. Adv. Mater. Sci.* **12**, 46–50 (2006)
57. T. Still, W. Cheng, M. Retsch, R. Sainidou, J. Wang, U. Jonas, N. Stefanou, G. Fytas, Simultaneous occurrence of structure-directed and particle resonance-induced phononic gaps in colloidal films. *Phys. Rev. Lett.* **100**, 194301 (2008)
58. T. Still, R. Sainidou, M. Retsch, U. Jonas, P. Spahn, G.P. Hellmann, G. Fytas, The “Music” of core-shell spheres and hollow capsules: influence of the architecture on the mechanical properties at the nanoscale. *Nano Lett.* **8**, 3194–3199 (2008)

59. T. Still, M. Retsch, U. Jonas, R. Sainidou, P. Rembert, K. Mpoukouvalas, G. Fytas, Vibrational eigenfrequencies and mechanical properties of mesoscopic copolymer latex particles. *Macromolecules* **43**, 3422–3428 (2010)
60. T. Still, G. Gantzounis, D. Kiefer, G. Hellmann, R. Sainidou, G. Fytas, N. Stefanou, Collective hypersonic excitations in strongly multiple scattering colloids. *Phys. Rev. Lett.* **106**, 175505 (2011)
61. D. Sutter-Widmer, P. Neves, P. Itten, R. Sainidou, W. Steurer, Distinct band gaps and isotropy combined in icosahedral band gap materials. *Appl. Phys. Lett.* **92**, 073308 (2008)
62. Y. Tanaka, Y. Tomoyasu, S. Tamura, Band structure of acoustic waves in phononic lattices: two-dimensional composites with large acoustic mismatch. *Phys. Rev. B* **62**, 7378–7393 (2000)
63. G. Wang, X.S. Wen, J.H. Wen, L.H. Shao, Y.Z. Liu, Two-dimensional locally resonant phononic crystals with binary structures. *Phys. Rev. Lett.* **93**, 154302 (2004)
64. W. Xiao, G.W. Zeng, Y.S. Cheng, Flexural vibration band gaps in a thin plate containing a periodic array of hemmed discs. *Appl. Acoust.* **69**, 255 (2008)
65. S. Yang, J.H. Page, Z. Liu, M.L. Cowan, C.T. Chan, P. Sheng, Focusing of sound in a 3D phononic crystal. *Phys. Rev. Lett.* **93**, 024301 (2004)
66. Z. Yang, H.M. Dai, N.H. Chan, G.C. Ma, P. Sheng, Acoustic metamaterial panels for sound attenuation in the 50–1000 Hz regime. *Appl. Phys. Lett.* **96**, 041906 (2010)
67. Z. Ye, H. Hsu, E. Hoskinson, Phase order and energy localization in acoustic propagation in random bubbly liquids. *Phys. Lett. A* **275**, 452–458 (2000)
68. J. Zhu, J. Christensen, J. Jung, L. Martin-Moreno, X. Yin, L. Fok, X. Zhang, A holey-structured metamaterial for acoustic deep-subwavelength imaging. *Nat. Phys.* **52**, 7 (2011)